Pseudostatic and Dynamic Nanomechanics of the Tunica Adventitia in Elastic Arteries Using Atomic Force Microscopy

Colin A. Grant and Peter C. Twigg*

Advanced Materials Engineering RKT Centre, School of Engineering, Design and Technology, University of Bradford, Bradford, Yorkshire BD7 1DP, U.K.

ABSTRACT Tunica adventitia, the outer layer of blood vessels, is an important structural feature, predominantly consisting of collagen fibrils. This study uses pseudostatic atomic force microscopy (AFM) nanoindentation at physiological conditions to show that the distribution of indentation modulus and viscous creep for the tunica adventitia of porcine aorta and pulmonary artery are distinct. Dynamic nanoindentation demonstrates that the viscous dissipation of the tunica adventitia of the aorta is greater than the pulmonary artery. We suggest that this mechanical property of the aortic adventitia is functionally advantageous due to the higher blood pressure within this vessel during the cardiac cycle. The effects on pulsatile deformation and dissipative energy losses are discussed.

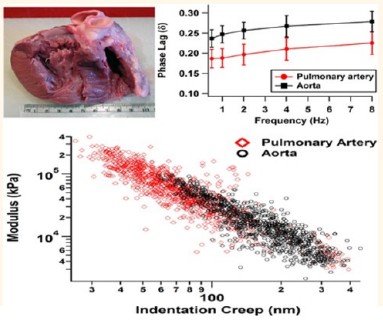

KEYWORDS: atomic force microscopy · artery · tunica adventitia · dynamic properties · nanomechanics

The biomechanical properties of arteries are an important factor in the overall function of the circulatory system. However, our understanding of how the structure and composition of arteries controls the biomechanics is poor and little is known about the properties of the discrete layers within these blood vessels.[1] Experimental studies of artery mechanics are traditionally based on the relationship between radial strain and blood pressure[2−5] and are therefore an examination of the vessels at a structural, rather than material, level. These studies are of limited value in modeling as they cannot be used to create generalized constitutive models. By applying nanomechanical testing techniques, such as atomic force microscopy (AFM) and nanoindentation, the mechanics of blood vessels can be investigated with very low test volumes and thus high spatial resolutions. These techniques allow variations in the mechanical properties of the different structural layers of blood vessels to be identified, giving a greater understanding of the overall vessel dynamics.

The elastic arteries originating from the left and right ventricles of the heart (aorta and pulmonary arteries, respectively) are critical to the fluid dynamics of the entire circulatory system. The left ventricle pumps oxygenated blood around the body, whereas, the right ventricle pumps deoxygenated blood to the lungs. The difference in function of the two ventricles leads to differences in form, most notably the increased muscle mass of the left ventricle, which can be seen by the thickness of the ventricular wall of a porcine heart in Figure 1a. Furthermore, the two arteries attached to the ventricles, as shown in Figure 1a, experience different pressures and stresses due their individual physiological function. As a result we might expect the mechanical properties of the blood vessels connected to these ventricles to be different.

Arteries and veins have structural similarities, where each comprises an endothelial inner wall (tunica intima), circularly arranged elastic fibres (tunica media) and an external wall (tunica adventitia). Artery structure differs, having an elastic lamina dispersed between layers of smooth muscle cells. The tunica adventitia provides an outer covering of the arteries and veins (Figure 1b). It is made of fibrous connective tissue (collagen and elastin), adipose tissue, nerve endings and cells (macrophages, mast, and fibroblasts),[7] that provides passive mechanical support,

* Address correspondence to p.twigg@bradford.ac.uk.

Received for review September 28, 2012 and accepted December 14, 2012.

Published online December 14, 2012
10.1021/nn304508x

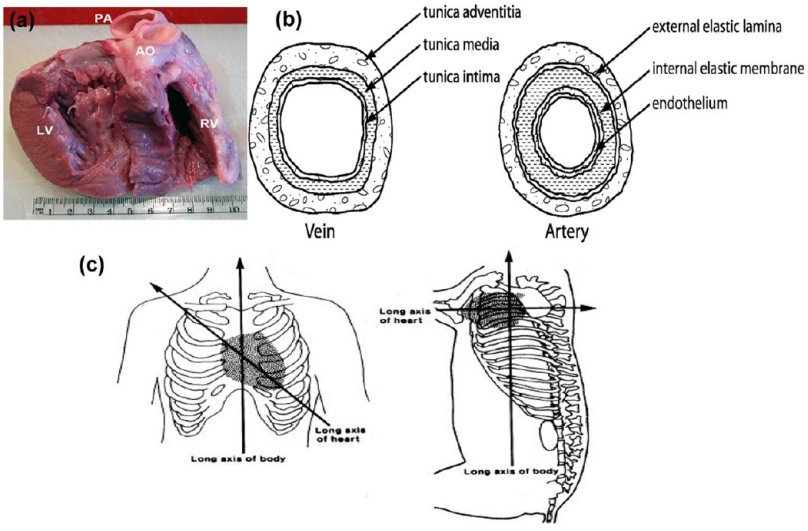

Figure 1. (a) Photograph of porcine heart showing aorta (AO), pulmonary artery (PA), and left (LV) and right (RV) ventricles. (b) Schematic of a cross section of vein and artery; (c) locations and variation of human and porcine heart orientation in gross anatomy. Reprinted with permission from ref 6. Copyright Wiley 1998.

limiting overdistension.[8] There is increasing experimental support that the adventitia has an important role in vascular processes, such as atherosclerosis and hypertensive remodelling.[9] This outer layer of collagenous fibres allows the blood vessels to stretch, preventing overexpansion due to the pressure exerted on the endothelial walls by pulsatile blood flow. Any excessive ballooning in the blood vessel walls that occurs at high systolic pressures may result in an abdominal aortic aneurysm, which involves large remodeling of the tunica adventitia.[10] Recent studies suggest that the adventitia has properties of a stem/progenitor cell niche in the artery wall that may be poised to respond to arterial injury.[11] The tunica adventitia also contains its own dynamic microvasculature, the *vasa vasorum*, which sustains the tunica media and provides a pathway for macrophage and leukocyte migration into the tunica intima. In addition, the tunica adventitia is in contact with other surrounding tissue and may actively contribute in exchange of signals and cells between the vessel wall and the tissue.[11] The collagen fibril orientation in tunica adventitia is largely circumferential, with a surface component of longitudinal fibrils.[12] The thickness of the tunica adventitia varies along its length, where its composition gives it strength and distensibility.[13] Vascular inflammation, which was commonly assumed to originate from the tunica intima and spread outward, is now considered to be initiated in the tunica adventitia and spreads inward.[10]

The atomic force microscope provides the ability to apply and measure nano- and pico-Newton forces on soft, biological materials in their native state,[14] coupled with the capacity to visualize structures as small as molecular bonds.[15] The highly inhomogeneous and hierarchical nature of biological tissues makes a multiscale approach to mechanical characterization, including nanoscale studies, particularly pertinent to these materials. In addition to improving our understanding of the mechanics of biological materials at the nanolevel, nanomechanical characterization of tissues has the potential to enhance the field of biomaterials, providing insights for novel materials and nanocomposites.[16]

A key aim of the multidisciplinary field of tissue engineering is the development of a functional substitute for damaged or diseased tissues and organs. There is a drive and ambition to develop a better mimetic for extracellular matrix (ECM); a nanoscale scaffold that promotes essential cellular processes and enhanced functional tissue organization.[17] The success of a tissue engineered arterial construct is largely dependent upon accurately mimicking the visco-elastic mechanics of the native tissue.[18]

Limited studies have been carried out on the mechanical properties of blood vessels at the nanolevel. Akhtar *et al.* examined the modulus of sections of aorta and vena cava, deducing that modulus was inversely correlated with elastic fiber density in the vein.[19] Ebenstein and Pruit used pseudostatic nanoindentation of agar and gelatin as a comparator with porcine aortic tissue.[20] One fascinating study used AFM nanoindentation of the tunica intima of an anaesthetized living rat to measure changes in nanomechanical modulus with chemically induced vasodilation and vasoconstriction.[21] Other related biomechanical work conducted using AFM include studies on coronary artery endothelium[22] and subendothelial matrix in bovine carotid artery.[1]

In this study we examine the nanomechanical and visco-elastic properties of the tunica adventitia of porcine blood vessels under physiological conditions, which to the best of our knowledge, have not been carried out before using AFM. Porcine tissue has been

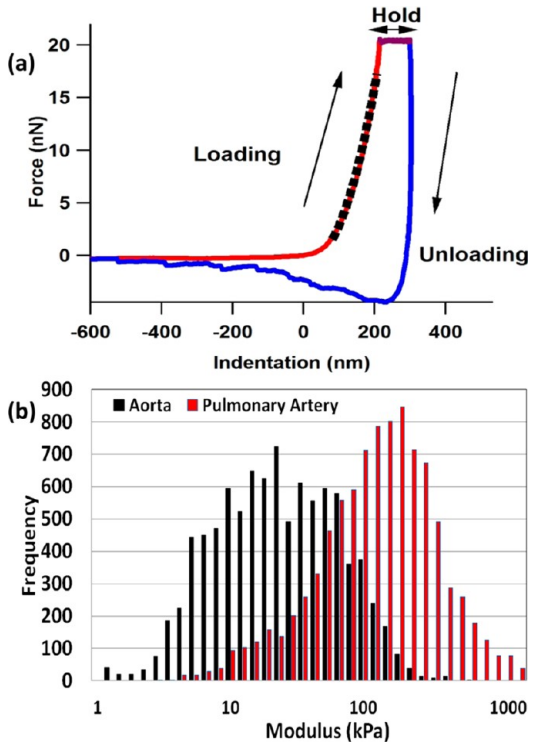

Figure 2. (a) Typical force plot showing loading, hold, and unloading sections, with corresponding theoretical fit (dotted line) to eq 1. (b) Modulus distribution of aorta and pulmonary artery sections (n = 9216 force plots per artery).

commonly used as a model in cardiovascular research, although there are some differences in anatomical structure, location and orientation between human and porcine hearts (Figure 1c).[6] Our study focuses on the pseudostatic and dynamic mechanics of this arterial outer structural layer, which is an important consideration for the development of tissue-engineered grafts. It is of considerable interest to determine how hierarchical assemblies and multicomposite layered structures define the mechanical behavior at the bulk, macro- and nanoscale.

RESULTS AND DISCUSSION

Static Nanoindentation. A typical force curve for the pulmonary artery, showing the three sections (load, hold, and unload) with the theoretical fit to eq 1, is shown in Figure 2a. The unloading section shows the removal of the entire applied load with minimal change in the indentation depth, suggesting some plastic deformation at the surface. As the tip is pulled away from the surface the tip−surface interaction becomes adhesive, gradually reducing with reducing contact area.

The modulus distributions of the two arteries are shown in Figure 2b, and appear to be log-normal, rather than a Gaussian bell shape. This is mainly due to the heterogeneity of the artery, even when using a 10 μm diameter sphere indenting probe. The range and median moduli are 0.7−391 and 15.8 kPa for the aorta; 2.3−1130 and 88.9 kPa for the pulmonary artery. A fresh AFM colloidal probe was used for the force mapping when changing from the aorta to the pulmonary artery tissue sections. The variation in the calibrated cantilever spring constant was approximately 4% (0.296 and 0.308 N/m), suggesting that the spring constant does not affect the recorded modulus distributions. The analysis and study of the tunica adventitia of porcine arteries, in realistic physiological conditions (fully hydrated and at 37 °C), using AFM nanoindentation techniques has not been covered in the literature to date, making a direct comparison of numbers difficult.

These results from nontargeted force maps of three sections of each artery show that the tunica adventitia of the pulmonary artery is on average stiffer than that of the aorta. We acknowledge that sampling and interpretation of mechanical data at the nanolevel can be complex, due to small localized anatomical variations that can occur through the 3D structure of the artery. AFM is a surface technique, where subsurface structures may not be visualized, but may influence nanomechanical properties. While this kind of nanomechanical analysis uses a linear elastic model eq 1 and is easily applied *via* most AFM software, its application is uncertain when indenting visco-elastic, anisotropic materials. However, for this investigation we only wish to use it as a subjective comparison between the two artery tissue types that originate from the same heart.

As our nanoindentation data have been obtained by sampling transverse sections of longitudinally aligned fibres we might expect the average modulus to approximate to a Voigt composite model. This effectively means that the macroscopic modulus for the tunica adventitia will be equal to the mean of the point modulus measurements, which are 25.8 kPa for the aorta and 128.6 kPa for the pulmonary artery. This result highlights the difference in stiffness between the two blood vessels, but also the low values compared to the literature. Akhtar *et al*. performed nanoindentation across the profile of ferret aorta, obtaining results of ~30 MPa for tunica adventitia regions and ~8 MPa for tunica intima.[19] Examining the anisotropic nature of the tissue, tensile testing on human tunica adventitia from the carotid artery, has been carried out, resulting in moduli of 1996 ± 867 and 1802 ± 703 kPa in the axial and circumferential directions respectively.[23] The high modulus values in both these studies are likely to be due, at least in part, to deviations from physiological conditions (full hydration and 37 °C). The mechanical and visco-elastic properties of soft biological matter are strongly dependent on the temperature, while dehydration can increase stiffnesses by orders of magnitude.[24] Other complexities when comparing biomechanical properties include differences in species, age, and health of the subject. However, we would not expect the mechanical properties of these tissues to be independent of length scale, due to the composite

nature of the tissue. The very small deformations elicited through nanoindentation will not stretch the fibres present enough for them to provide the reinforcing effect seen in macroscopic testing.

It is inevitable that the act of removal of anatomical tissue for *in vitro* testing will have an impact on biomechanical properties, and thus *in vivo* testing becomes an attractive method of biomechanical characterization. Macroscopic stiffnesses from *in vivo* testing of human aorta are reported to average 52.6 kPa,[25] which is close to our results reported here. A noninvasive ultrasound technique has been applied to human carotid arteries, using a nonlinear, hyper-elastic model giving a modulus of ~180 kPa for the tunica adventitia.[26] *In vivo* studies are generally based on blood pressure and radial strain of the blood vessel. The stiffnesses obtained from these studies are not material properties as they are dependent on the ratio between the blood vessel diameter and its thickness (from simple elastic deformation theory for thin walled cylinders under internal pressure). While *in vivo* measurements can be a useful parameter to monitor the health of the tissue, they are generally dependent on the blood vessel dimensions as well as its material properties.

To understand the complex response of the blood vessel mechanics at the nanolevel, it is important to consider the nature of its nanolevel structural components. The nanomechanical properties of individual collagen fibrils (100−200 nm diameter), the key constituent of the tunica adventitia, are known to vary by 3 orders of magnitude due to hydration[27] and can be "tuned" by varying the solvent, salinity, and pH.[28] Such subtle nanomechanical differences were readily detected using AFM and can be related to molecular structures and their interactions. The other key component of collagenous tissue is the ground substance (largely proteoglycans and water). As the ground substance is much softer than the collagen fibrils, it will be the dominating factor in the deformation behavior at such low loads. By using specific enzymes to remove the collagen phase of aortic tissue, AFM nanoindentation on the tunica adventitia showed a stiffness reduction by a factor of 50 times, peaking in the region of ~10 kPa.[29] Nanomechanical experimentation on the episclera (outer layer of the sclera) showed a distribution of moduli between its two components; proteoglycan matrix (~20 kPa) and collagen fibrils (~1.8 MPa).[30] These materials properties at the nanolevel can then form the basis for macroscopic mechanical models of the tissues, which take account of the inhomogeneous, hierarchical, composite nature of the biological structures, given a suitable theoretical framework.

The variation of biomechanical properties of collagenous tissue following freezing/defrosting still remains a debated issue.[31−33] In terms of artery tissue, Chow *et al.*, investigated the changes in the mechanical properties of aorta, by biaxial tensile testing, following

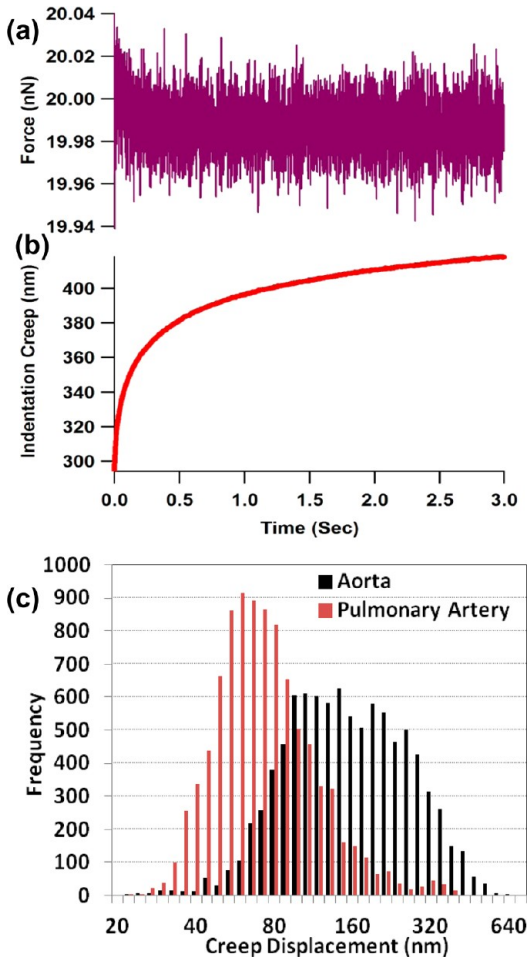

Figure 3. (a) Force *vs* time curve showing a constant load over the hold section with (b) its corresponding indentation *vs* time curve showing an indentation creep of ~130 nm. (c) Distribution of creep data collected for the two artery types (n = 9216 force plots for each artery).

freezing.[34] Here, the authors related changes in the tensile properties to a decrease in the content of soluble and insoluble collagen in the aorta, although the amount of cross-linked collagen remained unchanged. Histological comparisons on frozen and native femoral artery samples showed that cell nuclei had been injured, but no overall significant damage to the structure of the ECM was observed.[35] Directly relevant nanoindentation work recently carried out showed a small, statistically insignificant increase of instantaneous modulus of porcine aortic artery following flash freezing in liquid nitrogen and storing at −80 °C for 3 weeks.[36]

Nanoindentation Creep. To supplement the linear elastic analysis of the approach force curves of the artery samples, a measurement of creep indentation over a fixed period of time (3 s) was made. This was used as a simple indicator of the degree of time-dependent deformation shown by the tissues. To make such a measurement, it is important that the applied load (20 nN) remains constant over the time period (Figure 3a).

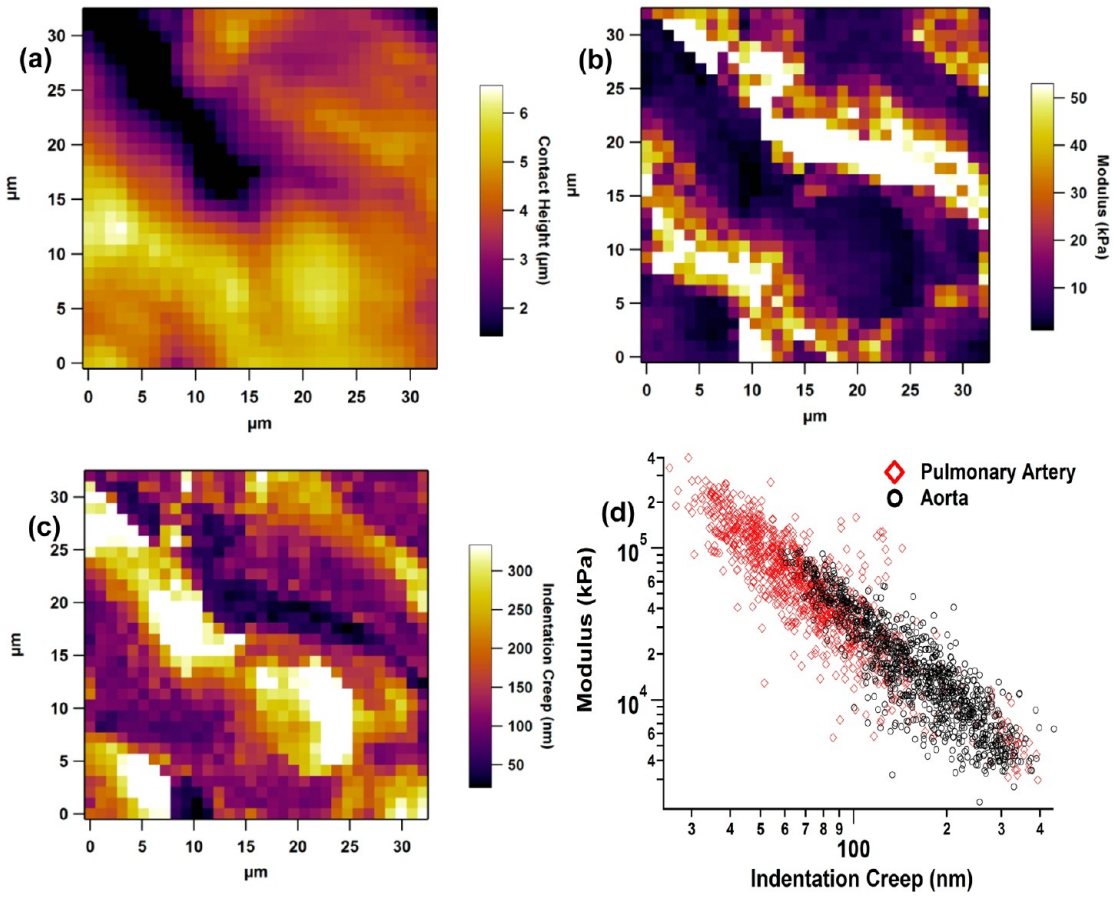

Figure 4. Force map made on the aorta tunica adventitia: (a) contact height, (b) modulus, (c) indentation creep, (d) scatter plot of modulus *vs* creep indentation from one force map (n = 1024 for each artery).

During the hold segment, the applied load was observed to fluctuate by no more than ~60 pN due to the active cantilever feedback control. The AFM monitors the continuing deformation of the tissue, giving the classic creep against time curve (Figure 3b). The maximum change in indentation creep over the 3 s period was calculated for each force curve on each tissue type. Comparisons of creep behavior between samples have been reported to be valid, provided they are assessed at the same holding time.[37]

As with the results from the modulus testing, the creep distributions are log-normal in nature (*cf.* Figures 2b and 3c). The indentation creep values for the aorta adventitia range from 22.1 to 632 nm with a median value of 147 nm, whereas for the pulmonary artery adventitia values range between 20.4 to 393 nm with a median of 67 nm. From these results, at a single hold period, the aorta tunica adventitia undergoes a greater amount of visco-elastic creep for the same given load. As the aorta is subjected to higher blood pressures than the pulmonary artery, having a structural visco-elastic outer layer (i.e., adventitia) to dampen and dissipate energy is a valuable function during cyclic pulsatile blood flow.

The surface of the sectioned arteries was too rough for high resolution scanning. This is likely to be caused

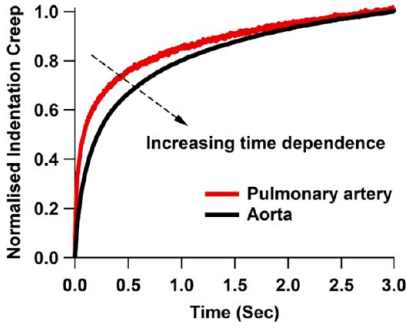

Figure 5. Representative normalized creep curves on each tunica adventitia (aorta τ_1 = 0.11, τ_2 = 1.24; pulmonary artery τ_1 = 0.07, τ_2 = 1.14).

by the relaxation of residual stresses within the blood vessels due to dissection, which may also reduce the nanomechanical stiffness compared with *in vivo* testing. Most AFM probes are in the region of 3 μm in height: anything over this value and the surface features will interfere with the cantilever probe assembly. AFM imaging of dehydrated sheep aorta samples has been previously demonstrated using ~5 μm thick tissue cryo-sections.[38] In our study, to visualize the surface the contact height of the spherical probe during force mapping was used as a contrast parameter (Figure 4a). As each pixel in the force map

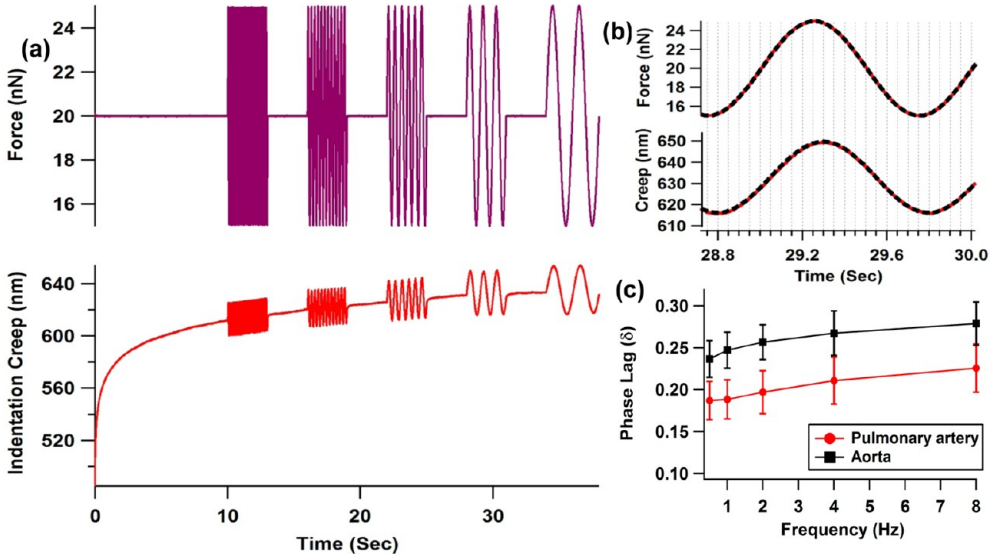

Figure 6. (a) Force (top) and indentation creep (bottom) *vs* time for dynamic loading; (b) close up on 1 Hz oscillation of force and creep with sinusoidal fitting (dashed line); (c) results for phase lag (radians) of two artery types; each marker is mean ± standard deviation (n = 100 force plots).

represents a single force plot, the contact height mapping can then be related to its corresponding modulus (Figure 4b) and creep (Figure 4c) map. The sampling force map size of $32 \times 32\ \mu m^2$ incorporates the middle third of the adventitial layer (~100 μm thick), which would avoid any possible issues with structural transitional changes at the adventitia/media interface. There does not appear to be any obvious relationship between the contact surface height and the modulus map. Comparing the lower half of Figure 4 panels a and b, there are regions of both low and high modulus with no large undulations in the height. However, the relationship between modulus and creep is reasonably clear, that is, regions of low modulus are directly correlated with regions of high creep. This suggests that the force curves from the regions of low modulus will inevitably include time-dependent deformation effects within the approach curves that are compounded with the elastic deformation. A scatter plot of modulus *vs* creep from a single force map made on both artery samples shows a slight overlapping in their behavior, while the negative gradient of the data highlights the inverse relationship between modulus and creep (Figure 4d). Hotelling's t-squared test was used to investigate the differences in creep and modulus for the two different tissue types. The test showed highly significant differences in means for the tunica adventitia of the aorta and pulmonary artery (F = 1588, $p < 0.0001$).

The subtle difference in the creep behavior of each adventitia can be further examined by normalizing representative creep data (Figure 5). Here, we have normalized the indentation creep data ($h(t)$) to vary between 0 and 1, before fitting a simple two exponent model ($h(t) = A_1 e^{-t/\tau_1} + A_2 e^{-t/\tau_2}$), where A_1 and A_2 are

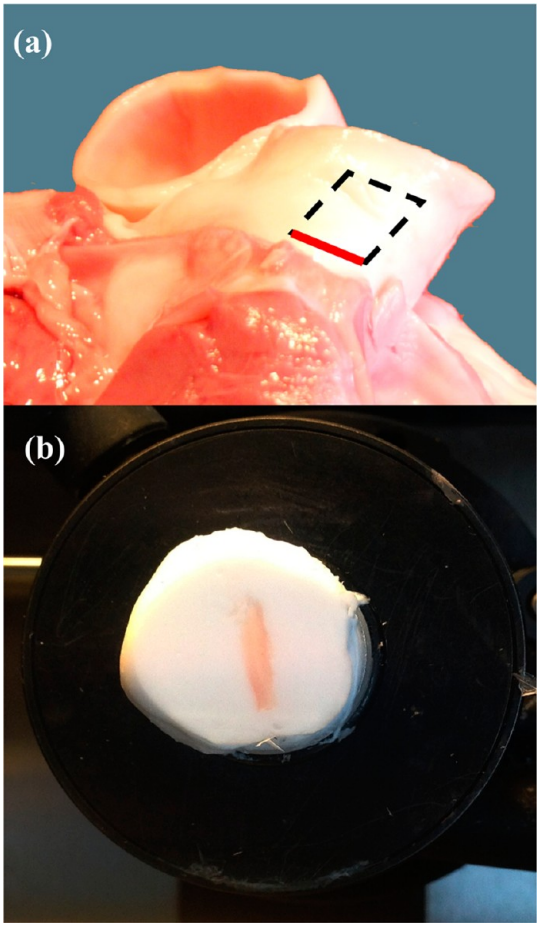

Figure 7. (a) Region of artery tissue on exposed outer face extracted for cryo-sectioning, dashed line. The face closest to the heart muscle is used for cryo-sectioning (solid red line). (b) Aorta sample in OCT medium for transverse cryo-sectioning, oriented so that the tunica adventitia is on the right side, tunica intima is on the left.

fitting constants, t is time and τ_1 and τ_2 are short and long-term relaxation times.

Differences in the normalized creep behavior can clearly be seen in Figure 5, where the aorta adventitia sample deforms much more slowly. This would demonstrate an increased time dependence, which has been previously seen in similar creep testing of a semicrystalline polymer at increasing temperatures.[39] AFM nanoindentation creep data have been subjected to mechanical modeling using springs and dashpots to describe such deformation behavior. This approach has been used on a range of materials including polymers,[40,41] lipid microbubbles,[24] cancer cells,[42] and bone.[37,43]

Dynamic Nanoindentation. A nanolevel dynamic mechanical analysis (DMA) approach to characterization provides a more robust way of investigating the viscoelastic nature of the tissues. The oscillatory force profile and its corresponding indentation creep are shown in Figure 6a, where a 10 s period of constant load is followed by the five experimental frequencies from 8 to 0.5 Hz. As the heart will pump at approximately between 0.6 and 3.6 Hz (i.e., 40 to 220 beats per minute), our experimental frequency range has physiological relevance. The oscillatory frequencies were applied in a decreasing manner to avoid excessive creep accumulation. A close-up of the recorded force and indentation creep at a frequency of 1 Hz is plotted in Figure 6b, together with their sinusoidal curve fittings. The measured strain (indentation) lags behind the applied stress (force), as expected for a visco-elastic material. The phase lag (δ) between the applied load and the measured indentation is recorded for each frequency, and results are shown in Figure 6c.

A phase lag of $\delta = 0$ would indicate a pure elastic response, and a phase lag of $\delta = \pi/2$ indicates a pure viscous response. For this experiment the tunica adventitia from the aorta sample had a higher degree of damping (*i.e.,* higher phase lag) than the pulmonary artery. Similar nanolevel DMA experimentation using AFM on human scar tissue was recently carried out and showed that the favorable damping properties found in healthy skin were not remodeled following wound healing.[44] The phase lag results in the aortic adventitia presented here are closely matched with those found in the upper dermis over a similar frequency range.[44] The structures and constituents of these tissues are reasonably similar; containing collagen, elastin and proteoglycans.

Cartilage is another collagen-based soft tissue that has been studied in a similar way. A frequency-dependent study on porcine cartilage using a dynamic nanoindentation technique was recently carried out at loads from 100 to 1000 μN.[45] Further, AFM based dynamic indentation has been carried out on native and proteoglycan depleted bovine cartilage at deformation length scales comparable to the fluid pore sizes, demonstrating poro-elastic behavior.[46] A further study by the same group compared AFM dynamic nanoindentation with finite element modeling,[47] highlighting that poro-elasticity is the dominant mechanism of the viscoelastic behavior of cartilage at the nanolevel. However, the collagen structure of arteries (collagen type I) is different from cartilage, which contains a network of collagen type II fibrils within a proteoglycan matrix.

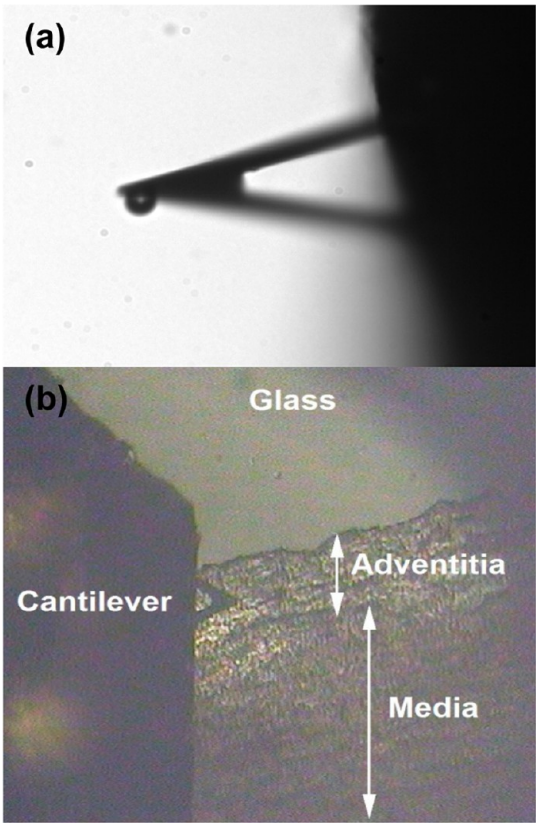

Figure 8. Light microscope images showing (a) the spherical AFM probe on the V-shaped cantilever location of the AFM cantilever (length = 100 μm) and (b) the cantilever positioned on the tunica adventitia region of the artery cross-section.

The proximity of the artery sections studied here, in relation to the heart muscle, means that they play a major role in determining the nature of the flow of blood through the circulatory system. Viscous damping of the pulsatile flow will act to smooth out pressure variations across the cardiac cycle. It has been shown that at physiological pressure the adventitia carries approximately 25% of the pressure load, and with higher pressures, this can increase to over 50% of the pressure load.[9] This would suggest that the damping role of the tunica adventitia of the aorta becomes even more important during periods of high blood pressure, as experienced during exercise, where the ventricle activity can reach over three beats per second. As the pulmonary artery experiences considerably less blood pressure, due to the relatively short distance from right ventricle to the lungs, the dissipation would be expected to be lower than that found in the tunica adventitia

of the aorta. The elasticity and viscosity of brachiocephalic arteries *in vivo* were affected by the removal of its adventitia, demonstrating that the adventitia plays an important role in the control of cardio-vascular function.[48]

CONCLUSIONS

In this work, the atomic force microscope has been used to determine the nanomechanical, visco-elastic properties of the tunica adventitia of two "elastic" arteries under physiological conditions (fully hydrated and at 37 °C). The tunica adventitia of both arteries exhibited distinctly different mechanical behavior, which can be linked to their function within the cardiovascular system. The adventitia from the aorta sample was more compliant, underwent greater visco-elastic creep, and exhibited more viscous dissipation than the pulmonary artery, over a physiologically relevant frequency range. Subtle differences exist in the creep curves of the arteries, demonstrating that the aortic adventitia had increased time-dependent behavior. As the aortic vessel has a higher internal blood pressure deriving from the stronger left ventricle, the demonstrated visco-elasticity of the tunica adventitia, at the nanolevel, may serve to moderate peaks in pressure pulses.

EXPERIMENTAL SECTION

Tissue Samples. A fresh porcine heart was obtained from a local abattoir/butchers (George Bolam & Sons, Sedgefield, UK), where the age of slaughtered pigs is approximately 6 to 9 months old. A square section (approx 8 mm × 8 mm) of artery tissue from the aorta and pulmonary artery was dissected, as close as possible to the entrance to the left and right ventricles on the two outer exposed sides of the aorta and pulmonary artery, as shown in Figure 7a.

Each artery tissue was embedded in OCT compound (Agar Scientific, UK), which is a polyethylene glycol-based medium that, upon freezing, provides a suitable substrate for preparing thin histological tissue sections (Figure 7b). The cut face closest to the heart muscle of each artery was placed upper most in the embedding compound. Each artery was sectioned in a cryostat (CM1510, Leica Microsystems, Germany), noting the orientation of the inner and outer aspects of the vessel. Transverse sections (12 μm thick) of the blood vessel tissue were cut and immediately pressed on to a polylysine coated microscope slide. Three sections from each tissue type were flash frozen in liquid nitrogen, stored in a −80 °C freezer and defrosted before use. Tissue samples were tested within one week of freezing.

AFM Nanomechanics. Microscope slides with the blood vessel sections were cut down and placed on a BioHeater stage of an MFP-3D AFM (Asylum Research, Santa Barbara, USA) before placing ~1.5 mL of ultrapure water (18.4 MΩ cm) on the surface and heating to 37 °C. A V-shaped silicon nitride cantilever with a 10 μm diameter glass sphere attached (Novascan, USA) was used throughout (Figure 8a). Following laser alignment, the cantilever was calibrated for laser sensitivity and spring constant ($k \approx 0.32$ N/m) using the thermal method[49] after 1 h equilibration time. Using the AFM's optical microscope (×10), the cantilever was moved to an arbitrary location in the center of the tunica adventitia (Figure 8b). The tunica adventitia was identified from the orientation of the cryo-section, but also by the transparency of this region in comparison with the darker, denser elastin fiber-rich tunica media.

Nanomechanical measurements were made by pressing the cantilever into the blood vessel wall in an organized array, or force map, of 32 × 32 indentations over a 32 μm scan area ($n = 1024$ force plots). Each indentation had a maximum load of $F_{max} = 20$ nN and a tip velocity of 4 μm/s. Three force maps were taken on the aortic tunica adventitia at random regions on a single tissue section, with each force map separated by at least 0.5 mm. Three fresh sections of aorta were tested; totalling $n = 9216$ individual nanoindentations. This routine was repeated using three sections from the pulmonary artery. Such a large number of force plots, under fully hydrated conditions and at body temperature, are required in order to give a realistic representation of the trends in mechanical and visco-elastic properties.

Elastic modulus was then estimated using a linear elastic Hertzian based theory for a spherical indenter:

$$E = \frac{3F(1-\nu^2)}{4\sqrt{R}}h^{3/2} \quad (1)$$

In this expression ν is the Poisson's ratio and is assigned a value of 0.5 (*i.e.*, incompressible), h is the indentation depth, and R is the radius of the indenting probe (5 μm).

Each indentation had a 3 s hold at maximum load, maintained by constant feedback on cantilever tip deflection. During this time, the visco-elastic biological tissue undergoes creep deformation. The amount of indentation creep during this hold period was recorded to give a measure of the tissue's time-dependent deformation.

Dynamic indentation was carried out to examine the visco-elastic properties of the two artery types. A single 10 × 10 force map, over a 32 μm scan size, was initiated at an arbitrary location in the tunica adventitia. Following loading ($F_{max} = 20$ nN, tip velocity of 4 μm/s), the cantilever was held at F_{max} for 10 s to allow creep equilibration before then undergoing 3 s periods of oscillatory motion at 8, 4, 2, 1, and 0.5 Hz, each separated by a 3 s hold. The force/indentation *vs* time curves were extracted and fitted to a sinusoidal curve ($y(t) = A\sin(\omega t + \delta)$), where ω is the angular frequency and δ is the phase difference.

Conflict of Interest: The authors declare no competing financial interest.

Acknowledgment. We would like to thank Professor D Tobin, Centre for Skin Sciences, University of Bradford, UK, for his expertise in histology sectioning. Elspeth Twigg, CORE IMS Ltd., is thanked for her help with the statistical analysis of the results.

REFERENCES AND NOTES

1. Peloquin, J.; Huynh, J.; Williams, R. M.; Reinhart-King, C. A. Indentation Measurements of the Subendothelial Matrix in Bovine Carotid Arteries. *J. Biomech.* **2011**, *44*, 815–821.
2. Boutouyrie, P.; Bussy, C.; Lacolley, P.; Girerd, X.; Laloux, B.; Laurent, S. Association between Local Pulse Pressure, Mean Blood Pressure, and Large-Artery Remodeling. *Circulation* **1999**, *100*, 1387–1393.
3. Cinthio, M.; Ahlgren, Å. R.; Bergkvist, J.; Jansson, T.; Persson, H. W.; Lindström, K. Longitudinal Movements and Resulting Shear Strain of the Arterial Wall. *Am. J. Physiol. Heart Circ. Physiol.* **2006**, *291*, H394–H402.
4. Kim, K.; Weitzel, W. F.; Rubin, J. M.; Xie, H.; Chen, X.; O'Donnell, M. Vascular Intramural Strain Imaging Using Arterial Pressure Equalization. *Ultrasound Med. Biol.* **2004**, *30*, 761–771.
5. Shing-Hong, L.; Chu-Chang, T.; Kang-Ming, C. A Novel Compliance Measurement in Radial Arteries using Strain-Gauge Plethysmography. *Physiol. Meas.* **2009**, *30*, 947–956.
6. Crick, S. J.; Sheppard, M. N.; Ho, S. Y.; Gebstein, L.; Anderson, R. H. Anatomy of the Pig Heart: Comparisons with Normal Human Cardiac Structure. *J. Anat.* **1998**, *193*, 105–119.
7. González, M. C.; Arribas, S. M.; Molero, F.; Fernández-Alfonso, M. S. Effect of Removal of Adventitia on Vascular Smooth Muscle Contraction and Relaxation. *Am. J. Physiol. Heart Circ. Physiol.* **2001**, *280*, H2876–H2881.

8. Rey, F. E.; Pagano, P. J. The Reactive Adventitia. *Artertioscler. Thromb. Vasc. Biol.* **2002**, *22*, 1962–1971.
9. Schulze-Bauer, C. A.; Regitnig, P.; Holzapfel, G. A. Mechanics of the Human Femoral Adventitia Including the High-Pressure Response. *Am. J. Physiol. Heart. Circ. Physiol.* **2002**, *282*, H2427–2440.
10. Maiellaro, K.; Taylor, W. R. The Role of the Adventitia in Vascular Inflammation. *Cardiovasc. Res.* **2007**, *75*, 640–648.
11. Majesky, M. W.; Dong, X. R.; Hoglund, V.; Mahoney, W. M.; Daum, G. The Adventitia: A Dynamic Interface Containing Resident Progenitor Cells. *Atertioscler. Thromb. Vasc. Biol.* **2011**, *31*, 1530–1539.
12. Smith, J. F. H.; Canham, P. B.; Starkey, J. Orientation of Collagen in the Tunica Adventitia of the Human Cerebral Artery Measured with Polarized Light and the Universal Stage. *J. Ultrastruct. Res.* **1981**, *77*, 133–145.
13. Ogeng'o, J.; Malek, A.; Kiama, S. Regional Differences in Aorta of Goat (*Capra Hircus*). *Folia Morphol. (Warsz).* **2010**, *69*, 253–257.
14. Hinterdorfer, P.; Dufrene, Y. F. Detection and Localization of Single Molecular Recognition Events Using Atomic Force Microscopy. *Nat. Methods* **2006**, *3*, 347–355.
15. Gross, L.; Mohn, F.; Moll, N.; Schuler, B.; Criado, A.; Guitián, E.; Peña, D.; Gourdon, A.; Meyer, G. Bond-Order Discrimination by Atomic Force Microscopy. *Science* **2012**, *337*, 1326–1329.
16. Kurland, N. E.; Drira, Z.; Yadavalli, V. K. Measurement of Nanomechanical Properties of Biomolecules Using Atomic Force Microscopy. *Micron* **2012**, *43*, 116–128.
17. Dvir, T.; Timko, B. P.; Kohane, D. S.; Langer, R. Nanotechnological Strategies for Engineering Complex Tissues. *Nat. Nanotechnol.* **2011**, *6*, 13–22.
18. Crapo, P. M.; Wang, Y. Physiologic Compliance in Engineered Small-Diameter Arterial Constructs Based on an Elastomeric Substrate. *Biomaterials* **2010**, *31*, 1626–1635.
19. Akhtar, R.; Schwarzer, N.; Sherratt, M. J.; Watson, R. E. B.; Graham, H. K.; Trafford, A. W.; Mummery, P. M.; Derby, B. Nanoindentation of Histological Specimens: Mapping the Elastic Properties of Soft Tissues. *J. Mater. Res.* **2009**, *24*, 638–646.
20. Ebenstein, D. M.; Pruitt, L. A. Nanoindentation of Soft Hydrated Materials for Application to Vascular Tissues. *J. Biomed. Mater. Res.* **2004**, *69*, 222–232.
21. Mao, Y.; Sun, Q.; Wang, X.; Ouyang, Q.; Han, L.; Jiang, L.; Han, D. *In Vivo* Nanomechanical Imaging of Blood-Vessel Tissues Directly in Living Mammals Using Atomic Force Microscopy. *Appl. Phys. Lett.* **2009**, *95*, 3704–3706.
22. Reichlin, T.; Wild, A.; Dürrenberger, M.; Daniels, A. U.; Aebi, U.; Hunziker, P. R.; Stolz, M. Investigating Native Coronary Artery Endothelium *in Situ* and in Cell Culture by Scanning Force Microscopy. *J. Struct. Biol.* **2005**, *152*, 52–63.
23. Teng, Z.; Tang, D.; Zheng, J.; Woodard, P. K.; Hoffman, A. H. An Experimental Study on the Ultimate Strength of the Adventitia and Media of Human Atherosclerotic Carotid Arteries in Circumferential and Axial Directions. *J. Biomech.* **2009**, *42*, 2535–2539.
24. Grant, C. A.; McKendry, J. E.; Evans, S. D. Temperature Dependent Stiffness and Visco-elastic Behaviour of Lipid Coated Microbubbles Using Atomic Force Microscopy. *Soft Matter* **2012**, *8*, 1321–1326.
25. Isnard, R. N.; Pannier, B. M.; Laurent, S.; London, G. M.; Diebold, B.; Safar, M. E. Pulsatile Diameter and Elastic Modulus of the Aortic Arch in Essential Hypertension: A Non-invasive Study. *J. Am. Coll. Cardiol.* **1989**, *13*, 399–405.
26. Khamdaeng, T.; Luo, J.; Vappou, J.; Terdtoon, P.; Konofagou, E. E. Arterial Stiffness Identification of the Human Carotid Artery Using the Stress–Strain Relationship *in Vivo*. *Ultrasonics* **2012**, *52*, 402–411.
27. Grant, C. A.; Brockwell, D. J.; Radford, S. E.; Thomson, N. H. Effects of Hydration on the Mechanical Response of Individual Collagen Fibrils. *Appl. Phys. Lett.* **2008**, *92*, 3902–3904.
28. Grant, C. A.; Brockwell, D. J.; Radford, S. E.; Thomson, N. H. Tuning the Elastic Modulus of Hydrated Collagen Fibrils. *Biophys. J.* **2009**, *97*, 2985–2992.
29. Beenakker, J. W. M.; Ashcroft, B. A.; Lindeman, J. H. N.; Oosterkamp, T. H. Mechanical Properties of the Extracellular Matrix of the Aorta Studied by Enzymatic Treatments. *Biophys. J.* **2012**, *102*, 1731–1737.
30. Grant, C. A.; Thomson, N. H.; Savage, M. D.; Woon, H. W.; Greig, D. Surface Characterisation and Biomechanical Analysis of the Sclera by Atomic Force Microscopy. *J. Mech. Behav. Biomed. Mater.* **2011**, *4*, 535–540.
31. Foutz, T. L.; Stone, E. A.; Abrams, C. F., Jr. Effects of Freezing on Mechanical Properties of Rat Skin. *Am. J. Vet. Res.* **1992**, *53*, 788–792.
32. Moon, D. K.; Woo, S. L. Y.; Takakura, Y.; Gabriel, M. T.; Abramowitch, S. D. The Effects of Refreezing on the Viscoelastic and Tensile Properties of Ligaments. *J. Biomech.* **2006**, *39*, 1153–1157.
33. Nazarian, A.; Hermannsson, B. J.; Muller, J.; Zurakowski, D.; Snyder, B. D. Effects of Tissue Preservation on Murine Bone Mechanical Properties. *J. Biomech.* **2009**, *42*, 82–86.
34. Chow, M.-J.; Zhang, Y. Changes in the Mechanical and Biochemical Properties of Aortic Tissue Due to Cold Storage. *J. Surg. Res.* **2011**, *171*, 434–442.
35. Venkatasubramanian, R.; Grassl, E.; Barocas, V.; Lafontaine, D.; Bischof, J. Effects of Freezing and Cryopreservation on the Mechanical Properties of Arteries. *Ann. Biomed. Eng.* **2006**, *34*, 823–832.
36. Hemmasizadeh, A.; Darvish, K.; Autieri, M. Characterization of Changes to the Mechanical Properties of Arteries Due to Cold Storage Using Nanoindentation Tests. *Ann. Biomed. Eng.* **2012**, *40*, 1434–1442.
37. Wu, Z.; Baker, T. A.; Ovaert, T. C.; Niebur, G. L. The Effect of Holding Time on Nanoindentation Measurements of Creep in Bone. *J. Biomech.* **2011**, *44*, 1066–1072.
38. Graham, H. K.; Hodson, N. W.; Hoyland, J. A.; Millward-Sadler, S. J.; Garrod, D.; Scothern, A.; Griffiths, C. E. M.; Watson, R. E. B.; Cox, T. R.; Erler, J. T.; *et al.* Tissue Section AFM: *In Situ* Ultrastructural Imaging of Native Biomolecules. *Matrix Biol.* **2010**, *29*, 254–260.
39. Grant, C. A.; Alfouzan, A.; Gough, T.; Twigg, P. C.; Coates, P. D. Nano-scale Temperature-Dependent Visco-elastic Properties of Polyethylene Terephthalate (PET) Using Atomic Force Microscope (AFM). *Micron* **2013**, *44*, 174–178.
40. Fischer-Cripps, A. C. A Simple Phenomenological Approach to Nanoindentation Creep. *Mater. Sci. Eng., A* **2004**, *385*, 74–82.
41. Yang, S.; Zhang, Y.-W.; Zeng, K. Analysis of Nanoindentation Creep for Polymeric Materials. *J. Appl. Phys.* **2004**, *95*, 3655–3666.
42. Moreno-Flores, S.; Benitez, R.; Vivanco, M.; Toca-Herrera, J. L. Stress Relaxation and Creep on Living Cells with the Atomic Force Microscope: A Means to Calculate Elastic Moduli and Viscosities of Cell Components. *Nanotechnology* **2010**, *21*, 445101.
43. Isaksson, H.; Nagao, S.; MaLkiewicz, M.; Julkunen, P.; Nowak, R.; Jurvelin, J. S. Precision of Nanoindentation Protocols for Measurement of Viscoelasticity in Cortical and Trabecular Bone. *J. Biomech.* **2010**, *43*, 2410–2417.
44. Grant, C. A.; Twigg, P. C.; Tobin, D. J. Static and Dynamic Nanomechanical Properties of Human Skin Tissue Using Atomic Force Microscopy: Effect of Scarring in the Upper Dermis. *Acta Biomater.* **2012**, *8*, 4123–4129.
45. Franke, O.; Göken, M.; Meyers, M. A.; Durst, K.; Hodge, A. M. Dynamic Nanoindentation of Articular Porcine Cartilage. *Mater. Sci. Eng., C* **2011**, *31*, 789–795.
46. Han, L.; Frank, E. H.; Greene, J. J.; Lee, H.-Y.; Hung, H.-H. K.; Grodzinsky, A. J.; Ortiz, C. Time-Dependent Nanomechanics of Cartilage. *Biophys. J.* **2011**, *100*, 1846–1854.
47. Nia, Hadi T.; Han, L.; Li, Y.; Ortiz, C.; Grodzinsky, A. Poroelasticity of Cartilage at the Nanoscale. *Biophys. J.* **2011**, *101*, 2304–2313.
48. Cabrera Fischer, E. I.; Bia, D.; Camus, J. M.; Zocalo, Y.; de Forteza, E.; Armentano, R. L. Adventitia-Dependent Mechanical Properties of Brachiocephalic Ovine Arteries in *in Vivo* and *in Vitro* Studies. *Acta Physiol.* **2006**, *188*, 103–111.
49. Hutter, J. L.; Bechhoefer, J. Calibration of Atomic-Force Microscope Tips. *Rev. Sci. Instrum.* **1993**, *64*, 1868–1873.